# Hierarchical Co-assembly-enabled 3D-Printing of Homogeneous and Heterogeneous Covalent Organic Frameworks

Mingshi Zhang,[†, ‡] Longyu Li,[†, ‡] Qianming Lin,[†] Miao Tang,[†] Yuyang Wu,[§] and Chenfeng Ke[†, *]

[†] Department of Chemistry, Dartmouth College, 41 College Street, Hanover, NH 03755

[§] IMSERC, Northwestern University, 2145 Sheridan Road, Evanston, IL 60208

*Supporting Information Placeholder*

**ABSTRACT:** Covalent organic frameworks (COFs) are crystalline polymers with permanent porosity. They are usually synthesized as micrometer-sized powders or two-dimensional thin films and membranes for applications in molecular storage, separation, and catalysis. In this work, we report a general method to integrate COFs with imine or β-ketoenamine linkages into three-dimensional (3D)-printing materials. A 3D printing template Pluronic F127 has been introduced to co-assemble with imine polymers in an aqueous environment. By limiting the degree of imine polycondensation during the COF formation, the amorphous imine-polymer and F127 form co-assembled 3D-printable hydrogels with suitable shear thinning and rapid self-healing properties. After the removal of F127 followed by an amorphous-to-crystalline transformation, three β-ketoenamine- and imine-based COFs have been fabricated into 3D monoliths, possessing high crystallinity, hierarchical pores with high surface areas as well as good structural integrity and robust mechanical stability. Moreover, when multiple COF-precursor inks are employed for 3D printing, heterogeneous dual-component COF monoliths are fabricated with high spatial precision. This method not only enables the development of COFs with sophisticated 3D macro-structure, it also facilitates the heterogeneous integration of COFs into devices with the interconnected interface at the molecular level.

Covalent organic frameworks (COFs),[1] especially imine and β-ketoenamine-linked COFs,[2] have demonstrated great promises for applications in molecular storage, separation, catalysis and energy storage due to their synthetic versatility, good chemical stability, high crystallinity, large void spaces, and accessible surface area. COFs are usually employed in the form of as-synthesized powders or 2D thin films[3] and membranes[4] to selectively adsorb and separate molecules of interest, benefiting from nano-sized pores defined by the periodically aligned molecular entities. The limited form factors of COF-based materials, however, posts challenges to expand their uses in complex 3D devices. Recently, 3D printing technology such as direct ink writing (DIW) has demonstrated promises for the fabrication of porous materials such as metal-organic frameworks (MOFs),[5] yet no COF-based 3D-printed material has been reported. Establishing a method to fabricate COF-based 3D-printed monoliths will not only allow for high-rate mass transfer of substrates at the macroscale[6] but also enable selective adsorption and catalytic conversion of substrates with suitable sizes at the nanoscale.[1e] Currently, the integration of these crystalline powders such as MOFs into 3D printing materials are achieved by forming MOF/polymer composites.[5] However, this approach possesses several intrinsic limitations: (1) the tradeoff between the mechanical stability, which requires larger binder amount, and the high surface area, which requires lower binder amount to avoid reducing[5a] or even blocking the nanosized pores of the fabricated monolith; (2) limited printability giving rise to the uncontrolled and uneven distribution[5c] of the porous particles; and (3) difficulties to integrate multiple porous materials with robust interfacial binding, since induvial porous material requires tailored polymer composition.

In this communication, we present the stepwise manipulation of the imine-COFs formation process[7] to introduce COFs, for the first time, as 3D-printing materials. Through a templated hierarchical co-assembly[8] followed by post-printing amorphous-to-crystalline network re-organization (Figure 1), crystalline single- and dual-component COF monoliths have been fabricated successfully. In our design, imine and β-ketoenamine-based COF precursors are polymerized in an aqueous environment in the presence of a supramolecular 3D printing template Pluronic F127, affording 3D-printable hydrogels composed of imine polymer/F127 co-assemblies[9] (Figure 1). The degree of polymerization (DP) of the amorphous

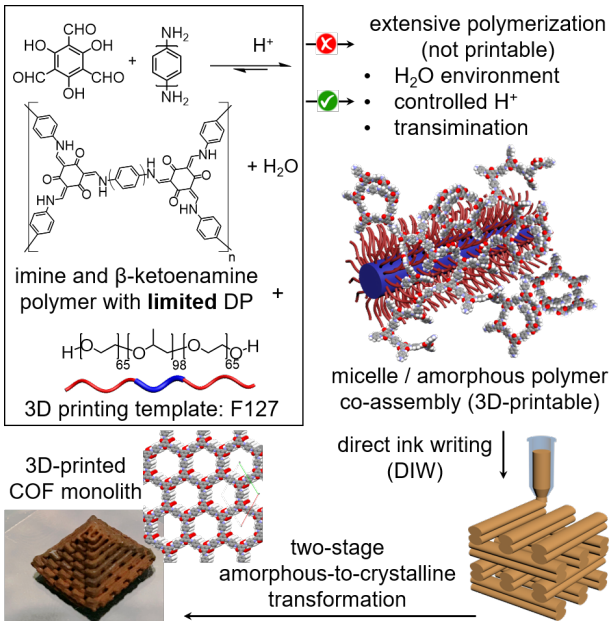


**Figure 1**. Design and synthesis of 3D-printed hierarchically porous imine and β-ketoenamine-linked COFs through a supramolecularly templated co-assembly process followed by a two-stage post-printing imine network transformation.

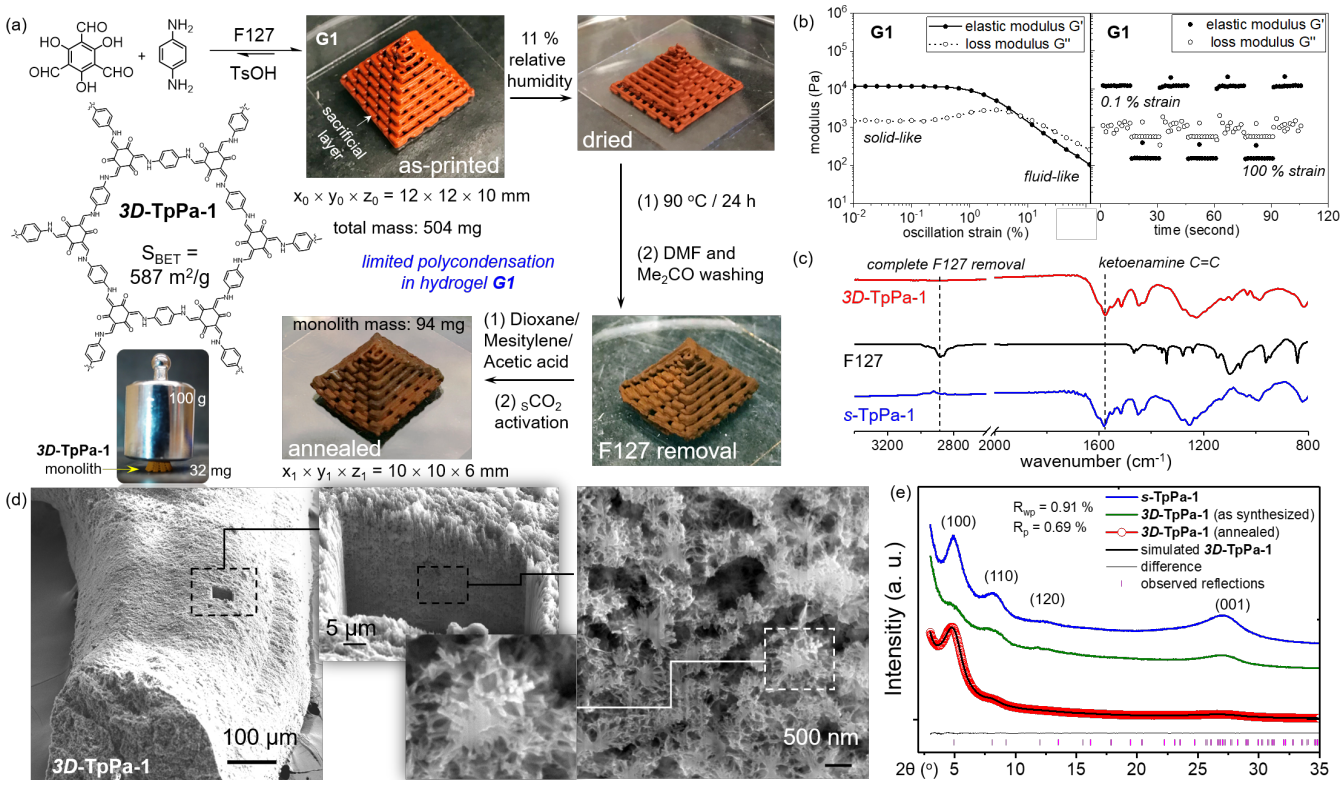


**Figure 2**. (a) Synthesis of ***3D*-TpPa-1** through Pluronic F127 templated co-assembly followed by post-printing framework re-organization. Inset: a robust ***3D*-TpPa-1** cubic lattice (32 mg) loaded with a 100 g weight. (b) Stress-strain (*left*) and step-strain (*right*) rheological measurements of hydrogel **G1**. (c) FT-IR spectra of ***s*-TpPa-1**, F127 and ***3D*-TpPa-1** respectively. (d) SEM images of a ***3D*-TpPa-1** and its focused ion beam sliced cross-section. Nano-crystalline fibers were observed in the cross-section. (e) PXRD profiles of ***s*-TpPa-1**, as synthesized ***3D*-TpPa-1** after F127 removal and annealed ***3D*-TpPa-1**, respectively.

imine (or β-ketoenamine) polymer is intentionally restrained by introducing a large excess of water, controlling the amount of acid catalyst and the introduction of a transimination step.[10] After 3D printing, the amorphous polymers are heated to extensively polymerize and re-organize the imine network. After the removal of F127 and solvent annealing, the 3D-printed COF-only monoliths possess homogeneous nano-to-macroscale hierarchical porous features, good structural integrity and mechanical robustness, and their measured surface areas match those of the correspondent COF powders. Furthermore, robust heterogeneous COF monoliths were obtained by 3D printing multiple hydrogels with different COF-precursors into designed 3D architectures. Benefiting from the reversible imine network formation, a molecular-level seamlessly interconnected interface is formed between two COFs, which cannot be achieved otherwise.

A β-ketoenamine COF **TpPa-1** reported[11] by Banerjee *et al.* was chosen as the model system because of its mild synthesis conditions and high chemical stability. Solution-phase synthesized **TpPa-1** (***s*-TpPa-1**) was obtained and its 2D hexagonal framework structure was confirmed by powder X-ray diffraction (PXRD) analysis. ***s*-TpPa-1** appear as irregular micrometer-sized particles under the scanning electron microscope (SEM, Figure S30), and its Brunauer-Emmett-Teller (BET) surface area was measured as 669 $m^2/g$ by $N_2$ sorption analysis (Figure S35). Physical blending of ***s*-TpPa-1** particles with F127 hydrogel affords a barely printable ink, which clogs the printer tips due to the coagulation of COF particles. The incomplete F127/***s*-TpPa-1** monolith possesses no measurable surface area, and its 3D architecture quickly collapsed into powders upon F127 removal (Figure S4). In order to achieve a 3D-printable COF with homogeneity across the nano-to-macroscale, we sought to co-assemble its amorphous polymer precursor with F127 micelles (Figure S20) to form viscoelastic hydrogels for DIW. Experimentally, a THF solution (25 mL) of 1,3,5-triformylphloroglucinol (**Tp**) (0.9 g, 4.3 mmol) and an aqueous solution (6 mL) of *p*-phenylenediamine (**Pa**, 0.7 g, 6.5 mmol), *p*-toluenesulfonic acid (TsOH, 0-2.6 mmol)[12] and Pluronic F127 (2.0 g) were mixed together. A majority of the THF was quickly evaporated in open air and the mixture gradually turned to a red-colored opaque F127/imine-polymer hydrogel **G1** (Figure 2a), indicating that the imine polycondensation was sufficiently restrained by the large excess of water so as to avoid precipitation. Stress-strain measurements of **G1** suggest an averaged elastic modulus of 12.0 kPa (Figure 2b, *left*), which is sufficient to support a high-profile 3D geometry. In the step-strain study (Figure 2b, *right*), **G1** deformed into a liquid-like material at 100% strain and immediately recovered its elastic modulus after the shear force removal, suggesting that **G1** possesses rapid self-healing property for 3D printing. Lattice pyramids (Figure 2a) with good structural integrity and stability were printed using **G1**. After DIW, the lattice was placed in a sealed chamber at 11 % relative humidity to gradually remove water and allow for an extensive imine polycondensation. Most of the water in the lattice was removed as indicated by the IR spectrum (Figure S17f) with 50% mass loss recorded. PXRD analysis of the freeze-dried gel (Figure S8) suggests that the periodically stacked hexagonal 2D framework had not yet been formed.

To extensively polymerize the imine network and initiate the amorphous-to-crystalline transformation, the lattice was heated to 90 °C for 24 h (Figure 2a), followed by intensive solvent washing to remove any unreacted species as well as the F127 template. The 3D architecture of the pyramid is well maintained after washing and a ~61 % mass loss was recorded in this step. In the IR spectra (Figure 2c), the $sp^3$ C-H stretching band at 2884 $cm^{-1}$ attributed to F127 disappeared after washing, suggesting a complete removal of F127. The C=C stretching band at 1580 $cm^{-1}$ suggests an extensive

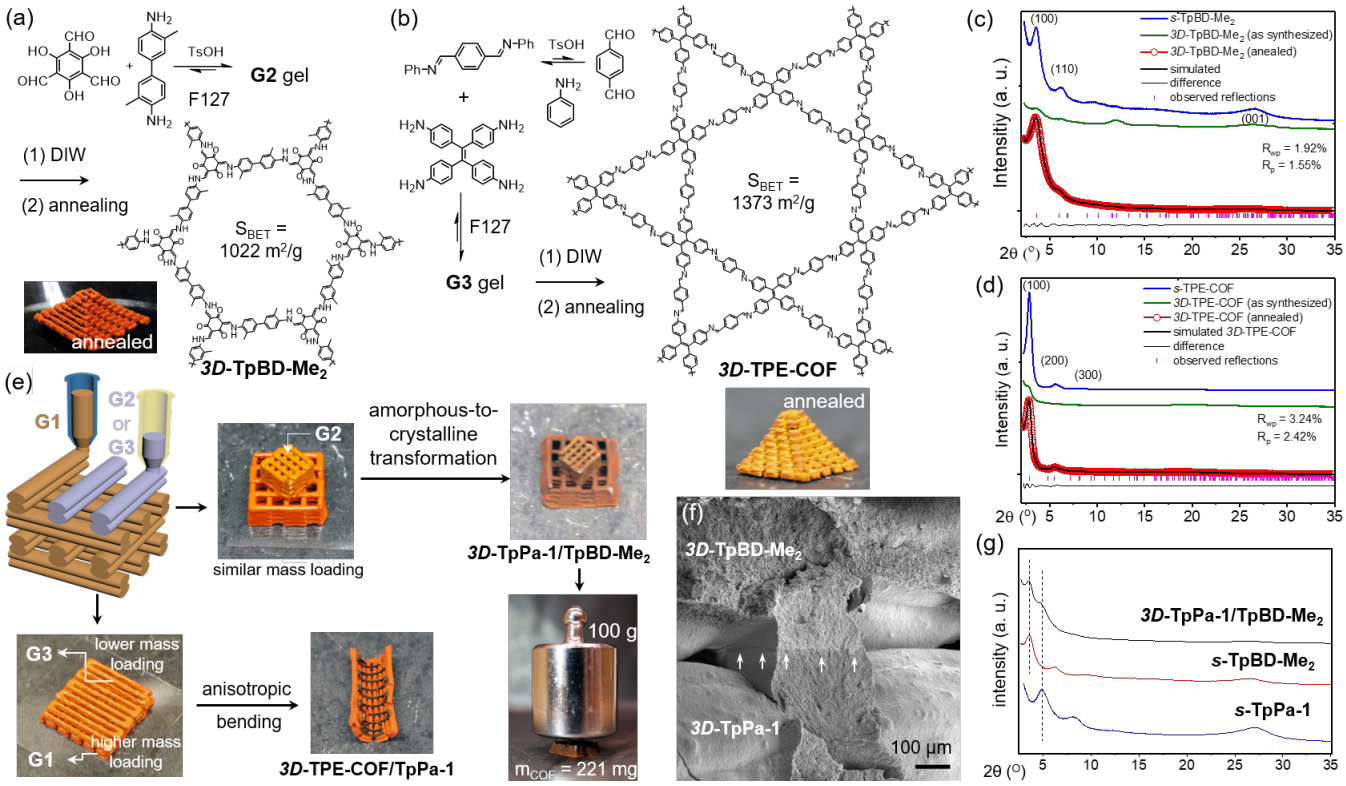


**Figure 3.** Synthesis of 3D-printed monoliths of ***3D*-TpBD-Me$_2$** (a) and ***3D*-TPE-COF** (b). (c) PXRD profiles of ***s*-TpBD-Me$_2$**, as synthesized and annealed ***3D*-TpBD-Me$_2$**, respectively. (d) PXRD profiles of ***s*-TPE-COF**, as synthesized and annealed ***3D*-TPE-COF**, respectively. (e) Dual-material 3D printing of heterogeneous COF monoliths and the obtained lattice of ***3D*-TpPa-1/TpBD-Me$_2$** and ***3D*-TpPa-1/TPE-COF**. No mechanical fracture was observed after placing 100 g weight on the ***3D*-TpPa-1/TpBD-Me$_2$** monolith (221 mg). (f) SEM image of an exposed interface formed between ***3D*-TpPa-1 and *3D*-TpBD-Me$_2$** in the printed heterogeneous monolith. (g) PXRD profiles of ***s*-TpPa-1**, ***s*-TpBD-Me$_2$**, and a 3D-printed heterogeneous monolith ***3D*-TpPa-1/TpBD-Me$_2$**, respectively.

imine-to-β-ketoenamine tautomerization. PXRD profile of the monolith suggests (Figure 2e) the formation of a moderately crystalline ***3D*-TpPa-1** with diffraction peaks of 2θ = 4.7°, 8.3°, 11.1°, and 26.5°. PXRD analysis of different samples obtained after F127 removal revealed that, increasing the heating time of the dried **G1** monolith from 24 h to 72 h and 120 h at 90 °C did not improve the monolith's crystallinity (Figure S9), nor did elevating the heating temperature to 120 or 150 °C (Figure S10). These results suggest that the network re-organization is hindered by the surrounding F127 matrix. However, we noticed that the amount of TsOH (0-2.6 mmol) added to the hydrogels had a significant impact on the crystallinity of the obtained ***3D*-TpPa-1** (Figure S11) and the stability of the 3D-printed architecture. While lower TsOH amount afforded as synthesized ***3D*-TpPa-1** with better crystallinity, higher TsOH amount allowed a more extensive β-ketoenamine polycondensation to form mechanically robust 3D architectures after solvent washing. An optimized TsOH (1.6 mmol) amount in the hydrogel was found to provide a balance in crystallinity and mechanical stability.

To improve the crystallinity of the as-synthesized ***3D*-TpPa-1** monolith, the lattice obtained after F127 removal was annealed in a dioxane/mesitylene/acetic acid (6M) mixture at 150 °C for 72 h. After annealing, the crystallinity of ***3D*-TpPa-1** improved significantly (Figure 2e, green to red), and the monoliths exhibited good structural integrity and outstanding mechanical robustness (Figure 2a, inset). Nitrogen adsorption isotherm (Figure S36) of the ***3D*-TpPa-1** acquired at 77 K suggests a BET surface area of 587 m$^2$/g, which matches that of the ***s*-TpPa-1** we synthesized. In the SEM experiments (Figure 2d), inter-connected nanocrystalline fibers were observed, which confirms the formation of crystalline COF throughout the monolith. Hierarchical porous features of the ***3D*-TpPa-1** monolith that attributed to the F127 removal were observed with pores ranging from a few nanometers to sub-micrometer throughout the dissected area of a 3D-printed lattice.

Following this method, another β-ketoenamine COF[11b] **TpBD-Me$_2$** and an imine-COF[13] **TPE-COF** were successfully integrated into DIW-compatible materials (Figure 3). Hydrogel **G2** formed by **Tp**, *o*-tolidine, F127 and TsOH were 3D-printed to lattice pyramid (Figure S26). Although the hexagonal framework has not been extensively formed after heating at 90 °C for 24 h (Figure 3c, green), a crystalline ***3D*-TpBD-Me$_2$** monolith was obtained after solvent annealing (Figure 3c, red), suggesting that the β-ketoenamine polymer still reorganizes its network after the removal of F127 matrix. The ***3D*-TpBD-Me$_2$** monolith possesses a measured BET surface area (1022 m$^2$/g, Figure S38) similar to that of solution-phase synthesized ***s*-TpBD-Me$_2$** (767 m$^2$/g, Figure S37). In the dissected SEM sample (Figure S32), similar crystalline fibrous structures were observed with hierarchical porous features generated after F127 removal. In contrast, mixing tetrakis(4-aminophenyl)ethene, terephthalaldehyde, and F127 in the absence or presence of TsOH did not afford a homogeneous hydrogel but a non-printable yellow precipitate, which gave rise to the rapid formation of large imine polymer particles. To decrease the DP of the imine polymer, aniline was introduced to form an imine intermediate (Figure 3b), which subsequently reacted with tetrakis(4-aminophenyl)ethene through a transimination[10] polymerization in the presence of F127. A 3D-printable hydrogel **G3** was obtained and 3D-printed into lattice pyramid. Upon heating and subsequent annealing under an $N_2$ atmosphere, a crystalline monolith ***3D*-TPE-COF** (Figure 3b) with a measured BET surface area of 1373 m$^2$/g (Figure S40) was obtained. PXRD (Figure 3d) and SEM analyses (Figure S33) suggest ***3D*-TPE-COF** possesses a periodically stacked 2D hexagonal framework at the nanoscale with hierarchical porous features.

The polymer network re-organization in these 3D-printed COF monoliths enables heterogeneous integration of different imine and β-ketoenamine COFs in a spatially defined 3D architecture. The cross-imination at the COF/COF interface would allow two COF materials to covalently connect to each other, therefore eliminating the binding issue in conventional fabrication methods.[14] Two heterogeneous lattice structures (Figure 3e) were 3D-printed using inks of **G1** and **G2**, and **G1** and **G3**, respectively. After the two-stage amorphous-to-crystalline transformation, mechanically robust dual-COF monolith ***3D*-TpPa-1/TpBD-Me$_2$** (Figure 3e) with high crystallinity (Figure 3g) were obtained. SEM studies revealed that two COFs are seamlessly bound at the COF/COF interface (Figure 3f), suggesting a molecular-level connection between the two COFs. To further demonstrate the strong interfacial binding between two COFs, the concentration of **TPE-COF** precursors in **G3** was intentionally kept significantly lower than that of **G1**. After annealing, the top layer composed of **TPE-COF** shrank more than the bottom layer composed of **TpPa-1**, forcing the heterogeneously 3D-printed monolith ***3D*-TpPa-1/TPE-COF** to bend into a half-round tubular structure (Figures 3e) at the macroscale, demonstrating the strong interfacial interaction between two COFs.

In summary, we have demonstrated a general method to integrate imine and β-ketoenamine COFs into 3D printing materials and fabricated the first set of single component and multi-component 3D-printed COF monoliths through hierarchical co-assembly enhanced direct-ink-writing, followed by two-stage post-printing network re-organization. At the nanoscale, the fabricated COF monoliths exhibit high crystallinity similar to their solution-phase synthesized COFs yet impart good mechanical robustness at the macroscale. Compared to the solution phase synthesized counterparts, these 3D-printed monoliths possess comparable measured surface areas and hierarchical porous features, which can potentially increase the mass transport rate for molecular storage, separation and catalysis. Furthermore, dual-COF monoliths with molecular-level structural integration at the COF/COF interfaces have been successfully fabricated using two COF-precursor inks. Our approach provides a facile method to fabricate homogeneous and heterogeneous COF monoliths with high crystallinity and designed macroscale 3D architectures, which will pave the way for future applications that require sophisticated 3D architectures.

## ASSOCIATED CONTENT

### Supporting Information

The Supporting Information is available free of charge on the ACS Publications website. Synthesis and characterizations (PDF)

## AUTHOR INFORMATION


### Corresponding Author

chenfeng.ke@dartmouth.edu

### Author Contributions

‡These authors contributed equally.


## ACKNOWLEDGMENT


We acknowledge funding support from the American Chemical Society Petroleum Research Fund (58377-DNI10), the National Science Foundation EPSCoR New Hampshire Bio-Made center (1757371) and the startup fund from Dartmouth College.


## REFERENCES


(1) (a) Huang, N.; Wang, P.; Jiang, D. Covalent organic frameworks: a materials platform for structural and functional designs. *Nat. Rev. Mater.* **2016**, *1*, 16068. (b) Bisbey, R. P.; Dichtel, W. R. Covalent organic frameworks as a platform for multidimensional polymerization. *ACS Cent. Sci.* **2017**, *3*, 533–543. (c) Diercks, C. S.; Yaghi, O. M. The atom, the molecule, and the covalent organic framework. *Science* **2017**, *355*, eaal1585. (d) Lohse, M. S.; Bein, T. Covalent organic frameworks: structures, synthesis, and applications. *Adv. Funct. Mater.* **2018**, *28*, 1705553. (e) Song, Y.; Sun, Q.; Aguila, B.; Ma, S. Opportunities of covalent organic frameworks for advanced applications. *Adv. Sci.* **2019**, *6*, 1801410.

(2) Ma, T.; Kapustin, E. A.; Yin, S. X.; Liang, L.; Zhou, Z.; Niu, J.; Li, L.-H.; Wang, Y.; Su, J.; Li, J.; Wang, X.; Wang, W. D.; Wang, W.; Sun, J.; Yaghi, O. M. Single-crystal X-ray diffraction structures of covalent organic frameworks. *Science* **2018**, *361*, 48–52.

(3) Zhao, Y.; Guo, L.; Gándara, F.; Ma, Y.; Liu, Z.; Zhu, C.; Lyu, H.; Trickett, C. A.; Kapustin, E. A.; Terasaki, O.; Yaghi, O. M. A Synthetic route for crystals of woven structures, uniform nanocrystals, and thin films of imine covalent organic frameworks. *J. Am. Chem. Soc.* **2017**, *139*, 13166–13172.

(4) Fan, H.; Gu, J.; Meng, H.; Knebel, A.; Caro, J. High-flux membranes based on the covalent organic framework COF-LZU1 for selective dye separation by nanofiltration. *Angew. Chem. Int. Ed.* **2018**, *57*, 4083–4087.

(5) (a) Thakkar, H.; Eastman, S.; Al-Naddaf, Q.; Rownaghi, A. A.; Rezaei, F. 3D-printed metal–organic framework monoliths for gas adsorption processes. *ACS Appl. Mater. Interfaces* **2017**, *9*, 35908–35916. (b) Kreider, M. C.; Sefa, M.; Fedchak, J. A.; Scherschligt, J.; Bible, M.; Natarajan, B.; Klimov, N. N.; Miller, A. E.; Ahmed, Z.; Hartings, M. R. Toward 3D printed hydrogen storage materials made with ABS-MOF composites. *Polym. Adv. Technol.* **2018**, *29*, 867–873. (c) Pei, P.; Tian, Z.; Zhu, Y. 3D printed mesoporous bioactive glass/metal-organic framework scaffolds with antitubercular drug delivery. *Microporous Mesoporous Mater.* **2018**, *272*, 24–30. (d) Lyu, Z.; Lim, G. J. H.; Guo, R.; Kou, Z.; Wang, T.; Guan, C.; Ding, J.; Chen, W.; Wang, J. 3D-printed MOF-derived hierarchically porous frameworks for practical high-energy density Li–O$_2$ batteries. *Adv. Funct. Mater.* **2019**, *29*, 1806658. (e) Sultan, S.; Abdelhamid, H. N.; Zou, X.; Mathew, A. P. CelloMOF: nanocellulose enabled 3D printing of metal–organic frameworks. *Adv. Funct. Mater.* **2019**, *29*, 1805372.

(6) Zhou, X.; Liu, C. Three-dimensional printing for catalytic applications: current status and perspectives. *Adv. Funct. Mater.* **2017**, *27*, 1701134.

(7) (a) Smith, B. J.; Overholts, A. C.; Hwang, N.; Dichtel, W. R. Insight into the crystallization of amorphous imine-linked polymer networks to 2D covalent organic frameworks. *Chem. Commun.* **2016**, *52*, 3690–3693. (b) Tan, J.; Namuangruk, S.; Kong, W.; Kungwan, N.; Guo, J.; Wang, C. Manipulation of amorphous-to-crystalline transformation: towards the construction of covalent organic framework hybrid microspheres with NIR photothermal conversion ability. *Angew. Chem. Int. Ed.* **2016**, *55*, 13979–13984.

(8) Li, L.; Zhang, P.; Zhang, Z.; Lin, Q.; Wu, Y.; Cheng, A.; Lin, Y.; Thompson, C. M.; Smaldone, R. A.; Ke, C. Hierarchical co-assembly enhanced direct ink writing. *Angew. Chem. Int. Ed.* **2018**, *57*, 5105–5109.

(9) Truby, R. L.; Lewis, J. A. Printing soft matter in three dimensions. *Nature* **2016**, *540*, 371–378.

(10) Vitaku, E.; Dichtel, W. R. Synthesis of 2D imine-linked covalent organic frameworks through formal transimination reactions. *J. Am. Chem. Soc.* **2017**, *139*, 12911–12914.

(11) (a) Kandambeth, S.; Mallick, A.; Lukose, B.; Mane, M. V.; Heine, T.; Banerjee, R. Construction of crystalline 2D covalent organic frameworks with remarkable chemical (acid/base) stability via a combined reversible and irreversible route. *J. Am. Chem. Soc.* **2012**, *134*, 19524–19527. (b) Karak, S.; Kandambeth, S.; Biswal, B. P.; Sasmal, H. S.; Kumar, S.; Pachfule, P.; Banerjee, R. Constructing ultraporous covalent organic frameworks in seconds via an organic terracotta process. *J. Am. Chem. Soc.* **2017**, *139*, 1856–1862.

(12) TsOH is limited below 0.6 *M* to form printable viscoelastic hydrogels at room temperature, since the critical gelation temperature of Pluronic F127 increases from ca. 4 ºC to 27 ºC and 37 ºC in the presence of 0, 0.6 and 1.0 *M* of TsOH, respectively, See Figure S22.

(13) (a) Zhou, T. Y.; Xu, S. Q.; Wen, Q.; Pang, Z. F.; Zhao, X. One-step construction of two different kinds of pores in a 2D covalent organic framework. *J. Am. Chem. Soc.* **2014**, *136*, 15885–15888. (b) Ascherl, L.; Sick, T.; Margraf, J. T.; Lapidus, S. H.; Calik, M.; Hettstedt, C.; Karaghiosoff, K.; Döblinger, M.; Clark, T.; Chapman, K. W.; Auras, F.; Bein, T. Molecular docking sites designed for the generation of highly crystalline covalent organic frameworks. *Nat. Chem.* **2016**, *8*, 310–316.

(14) Bétard, A.; Fischer, R. A. Metal–organic framework thin films: from fundamentals to applications. *Chem. Rev.* **2012**, *112*, 1055–1083.

Table of Contents